

Tuning pure out-of-plane piezoelectric effect of penta-graphene: a first-principle study

San-Dong Guo

School of Electronic Engineering, Xi'an University of Posts and Telecommunications, Xi'an 710121, China

For two-dimensional (2D) materials, a pure large out-of-plane piezoelectric response, compatible with the nowadays bottom/top gate technologies, is highly desired. In this work, the piezoelectric properties of penta-graphene (CCC) monolayer are studied with pure out-of-plane piezoelectric effect by density functional theory (DFT). However, the d_{36} is very small, and only -0.065 pm/V. Two strategies are proposed to enhance piezoelectric properties of CCC monolayer. Firstly, both biaxial and uniaxial strains are applied, but the enhancement is very small, and at -2% biaxial (-4% uniaxial) strain, the d_{36} is increased only by 3.1% (13.9%). Secondly, a Janus penta-monolayer (CCB) is constructed by replacing the top C (B) atomic layer in monolayer CCC [pentagonal CB_2 monolayer (CBB)] with B (C) atoms, which shows dynamic and mechanical stability. Fortunately, the pure out-of-plane piezoelectric effect of CCB monolayer still holds, and exhibits a band gap. The calculated d_{31} and d_{32} are -0.505 pm/V and 0.273 pm/V, respectively, which are very larger than d_{36} of CCC monolayer. The out-of-plane piezoelectricity d_{31} of CCB monolayer is obviously higher compared with many other 2D known materials. Moreover, its room-temperature electronic mobility along y direction is as high as $8865.23 \text{ cm}^2\text{V}^{-1}\text{s}^{-1}$. Our works provide a new way to achieve pure out-of-plane piezoelectric effect, which is highly desirable for ultrathin piezoelectric devices.

PACS numbers: 71.20.-b, 77.65.-j, 72.15.Jf, 78.67.-n

Email:sandongyuwang@163.com

Keywords: Penta-graphene, Piezoelectronics, 2D materials,

I. INTRODUCTION

Beyond graphene, a large amount of 2D carbon allotropes have been investigated. The CCC monolayer of them, composed entirely of carbon pentagons, could be realized experimentally with good thermodynamic stability¹. Inspired from CCC monolayer, other pentagon-based 2D materials have been theoretically predicted or experimentally synthesized, such as penta- CB_2 ², penta- SnX_2 ($\text{X}=\text{S}, \text{Se}, \text{or Te}$)³ and penta- AlN_2 ⁴. The mechanical behavior of monolayer CCC under multi-axial loading has been studied by DFT calculations, and the structure has lower ultimate tensile strength compared to graphene⁵. The phonon transport properties of CCC monolayer have been widely investigated theoretically, and the intrinsic lattice thermal conductivity is significantly reduced as compared to that of graphene⁶⁻⁸. The magnetic moments can be induced by an isolated hydrogen atom absorbed on CCC monolayer, which changes CCC monolayer from a semiconductor to half-metallic⁹. However, to the best of our knowledge, piezoelectric properties of CCC monolayer haven't been reported.

In fact, the piezoelectricity in 2D materials has attracted growing interest¹⁰ because of potential nanoscale piezoelectric applications, like sensors, actuators and energy sources. For 2D materials, the reduction in dimensionality makes their inversion symmetry disappear, which allows them to become piezoelectric. Experimentally, the monolayer MoS_2 with the 2H phase has been proved to be piezoelectric ($e_{11}=2.9\times 10^{-10} \text{ C/m}$)^{11,12}, and the existence of vertical dipoles in the Janus MoSSe monolayer has also been observed, showing an intrinsic vertical piezoelectric response¹³. In theory, lots of studies on piezoelectric properties related with 2D materials have been reported¹⁴⁻¹⁸, like transition metal dichalcogenides

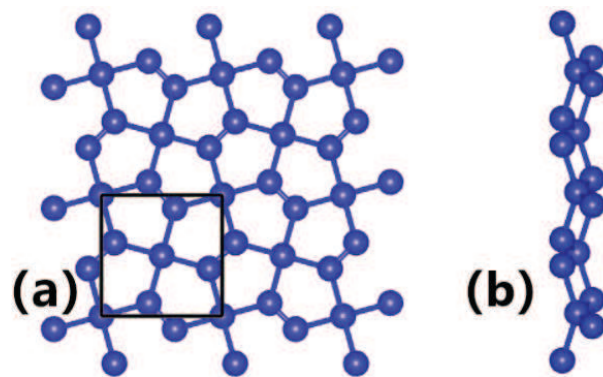


FIG. 1. (Color online) The crystal structure of penta-graphene: top view (a) and side view (b), and the primitive cell is marked by black line.

(TMD), group IIA and IIB metal oxides, group III-V semiconductors, group-V binary semiconductors and Janus TMD. It is surprising that the giant piezoelectricities in monolayer SnSe , SnS , GeSe and GeS have been predicted by the first-principle calculations¹⁶, as high as $75\text{-}251$ pm/V along the the armchair direction. Some 2D materials only exhibit an in-plane piezoelectricity, like TMD monolayers¹⁵, and an additional out-of-plane piezoelectricity has been observed in many 2D materials, like Janus TMD¹⁴. A pure large out-of-plane piezoelectric response is highly desired, which is compatible with the nowadays bottom/top gate technologies. However, the pure out-of-plane piezoelectric response in 2D materials is rarely reported.

In this work, the piezoelectric properties of CCC monolayer are reported by using density functional perturbation theory (DFPT)¹⁹ with generalized gradient approx-

imation (GGA). Only out-of-plane d_{36} exists for CCC monolayer, but it is very small. Both biaxial and uniaxial strains are used to tune its piezoelectric properties, but the improvement is very small. Janus monolayer can be built from symmetric sandwich structure, like MoSSe synthesized by replacing the top S atomic layer in MoS₂ with Se atoms¹³. Inspiring from MoSSe monolayer, a Janus CCB monolayer with dynamic and mechanical stability is constructed, and the special symmetry leads to only out-of-plane piezoelectric effect. Compared with d_{36} of CCC monolayer, the predicted d_{31} and d_{32} obviously are improved, the d_{31} of which is higher compared with other many 2D known materials. Another significant advantage for CCB monolayer is a very high room-temperature electronic mobility (8865.23 cm²V⁻¹s⁻¹) along y direction. Therefore, our works give an experimental proposal to achieve pure out-of-plane piezoelectricity in 2D materials, and pave a way for designing piezoelectric devices compatible with the nowadays bottom/top gate technologies.

The rest of the paper is organized as follows. In the next section, we shall give our computational details and methods about piezoelectric coefficients. In the third and fourth sections, we shall present piezoelectric properties of monolayer CCC and CCB. Finally, we shall give our conclusions in the fifth section.

II. COMPUTATIONAL DETAIL

Within the framework of DFT²⁰, our calculations are performed by using the VASP package^{21–23}. The projected augmented wave (PAW) method with a kinetic cutoff energy of 500 eV is adopted, and we use the popular GGA of Perdew, Burke and Ernzerhof (GGA-PBE)²⁴ as the exchange-correlation potential. For all studied monolayers, a vacuum spacing of more than 16 Å along the z direction is included to avoid interactions between two neighboring images. The total energy convergence criterion is set to 10⁻⁸ eV, and the Hellmann-Feynman forces on each atom are less than 0.0001 eV.Å⁻¹. The coefficients of the elastic stiffness tensor C_{ij} are calculated by using the finite difference method (FDM), and the piezoelectric stress coefficients e_{ij} are calculated by DFPT method¹⁹. Within FDM and DFPT, the electronic and ionic contribution to the elastic and piezoelectric stress coefficient can be attained directly from VASP code. For C_{ij} and e_{ij} , the Brillouin zone sampling is done using a Monkhorst-Pack mesh of 23×23×1 for CCC monolayer and CBB monolayer, and 18×19×1 for CCB monolayer. The 2D elastic coefficients C_{ij}^{2D} and piezoelectric stress coefficients e_{ij}^{2D} have been renormalized by the length of unit cell along z direction (Lz): $C_{ij}^{2D} = Lz C_{ij}^{3D}$ and $e_{ij}^{2D} = Lz e_{ij}^{3D}$.

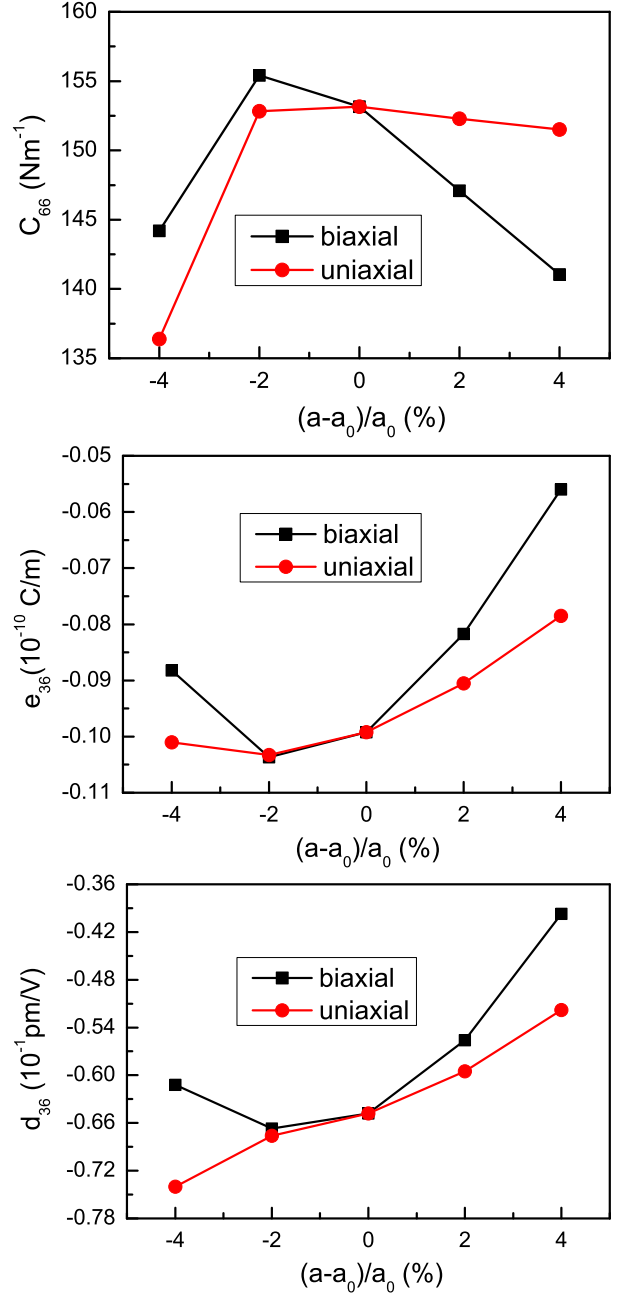


FIG. 2. (Color online) For monolayer CCC, the elastic constants C_{66} , piezoelectric coefficients e_{36} and d_{36} with the application of biaxial and uniaxial strains.

III. PIEZOELECTRIC PROPERTIES OF CCC MONOLAYER

The strain or stress can induce a change of polarization in noncentrosymmetric crystals, described by the third-rank piezoelectric stress tensors e_{ijk} and strain tensor d_{ijk} . They from the sum of ionic and electronic contributions are defined as:

$$e_{ijk} = \frac{\partial P_i}{\partial \varepsilon_{jk}} = e_{ijk}^{elc} + e_{ijk}^{ion} \quad (1)$$

TABLE I. For CCC, CCB and CBB monolayers, the lattice constants a_0/b_0 (Å) and γ , the GGA gaps (eV), and the elastic constants C_{ij} (Nm⁻¹).

| Name | a_0/b_0 | γ | Gap | C_{11} | C_{22} | C_{12} | C_{66} |
|------|-----------|----------|------|----------|----------|----------|----------|
| CCC | 3.639 | 90 | 2.20 | 271.84 | 271.84 | -20.86 | 153.15 |
| CCB | 3.771 | 92.107 | 0.66 | 142.36 | 193.07 | 34.40 | 61.71 |
| CBB | 3.933 | 90 | 1.41 | 86.78 | 86.78 | 87.86 | 89.20 |

TABLE II. For CCC, CCB and CBB monolayers, piezoelectric coefficients e_{ij} and d_{ij} , along with out-of-plane piezoelectric coefficients of some typical 2D materials, like SbTeI³⁴, BiTeI³⁴, MoSSe³³ and MoSTe³⁵. The unit is 10⁻¹⁰C/m for e_{ij} (pm/V for d_{ij}).

| Name | e_{31} | d_{31} | e_{32} | d_{32} | e_{36} | d_{36} |
|-------|----------|----------|----------|----------|----------|----------|
| CCC | | | | | -0.099 | -0.065 |
| CCB | -0.624 | -0.505 | 0.353 | 0.273 | | |
| CBB | | | | | -0.372 | -0.418 |
| SbTeI | -0.13 | -0.37 | -0.13 | -0.37 | | |
| BiTeI | -0.23 | -0.66 | -0.23 | -0.66 | | |
| MoSSe | 0.42 | 0.29 | 0.42 | 0.29 | | |
| MoSTe | 0.5 | 0.4 | 0.5 | 0.4 | | |

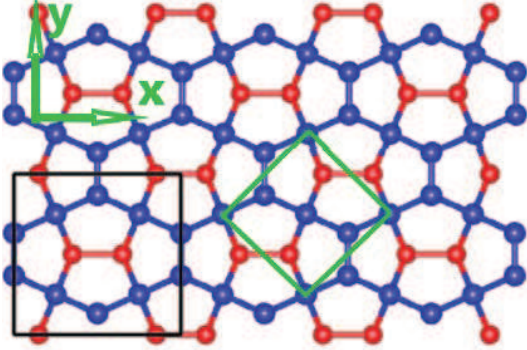


FIG. 3. (Color online) The top view of crystal structure of CCB, and the primitive cell and rectangle supercell are marked by green and black lines, respectively.

and

$$d_{ijk} = \frac{\partial P_i}{\partial \sigma_{jk}} = d_{ijk}^{elc} + d_{ijk}^{ion} \quad (2)$$

Where P_i , ε_{jk} and σ_{jk} are polarization vector, strain and stress, respectively. By employing Voigt notation, for 2D materials with only considering in-plane strain components¹⁴⁻¹⁸, the d_{ij} can be derived using the relation:

$$\begin{pmatrix} e_{11} & e_{12} & e_{16} \\ e_{21} & e_{22} & e_{26} \\ e_{31} & e_{32} & e_{36} \end{pmatrix} = \begin{pmatrix} d_{11} & d_{12} & d_{16} \\ d_{21} & d_{22} & d_{26} \\ d_{31} & d_{32} & d_{36} \end{pmatrix} \begin{pmatrix} C_{11} & C_{12} & C_{16} \\ C_{21} & C_{22} & C_{26} \\ C_{61} & C_{62} & C_{66} \end{pmatrix} \quad (3)$$

Where the C_{ij} is elastic tensor, which can be calculated by FDM, and the e_{ij} can be attained by DFPT. The CCC monolayer has $P42_1m$ symmetry (space group number 113), and the corresponding point group $42m$ makes Equation 3 become:

$$\begin{pmatrix} 0 & 0 & 0 \\ 0 & 0 & 0 \\ 0 & 0 & e_{36} \end{pmatrix} = \begin{pmatrix} 0 & 0 & 0 \\ 0 & 0 & 0 \\ 0 & 0 & d_{36} \end{pmatrix} \begin{pmatrix} C_{11} & C_{12} & 0 \\ C_{12} & C_{11} & 0 \\ 0 & 0 & C_{66} \end{pmatrix} \quad (4)$$

Here, the d_{36} is derived by Equation 4:

$$d_{36} = \frac{e_{36}}{C_{66}} \quad (5)$$

It is clearly seen that only out-of-plane piezoelectric effect can be observed.

The penta-graphene can be considered as a sandwich structure, with the 4-coordinated C atoms sandwiched between the 3-coordinated atoms, and the schematic structure is plotted in Figure 1. Firstly, the lattice constants of CCC are optimized ($a=b=3.639$ Å), which is very close to previous theoretical values¹. The elastic stiffness coefficients C_{ij} and piezoelectric stress tensors e_{ij} are calculated, and then d_{ij} can be attained. By using FDM, we obtain $C_{11}=271.84$ Nm⁻¹ $C_{12}=-20.86$ Nm⁻¹ and $C_{66}=153.15$ Nm⁻¹. The calculated C_{ij} agree well with previous ones¹. The C_{12} is negative, which means a negative Poisson's ratio. These related data are listed Table I. For 2D materials, a pure out-of-plane piezoelectric response, compatible with the nowadays bottom/top gate technologies, is highly desired. For CCC monolayer, only out-of-plane piezoelectric response exists, but the predicted piezoelectric coefficient d_{36} is very small, and the calculated value: $e_{36}=-0.099 \times 10^{-10}$ C/m and $d_{36}=-0.065$ pm/V. Some strategies should be applied to improve piezoelectric effect of CCC monolayer, and that only out-of-plane piezoelectric response holds.

It has been proved that strain can effectively improve the piezoelectric response of 2D materials, such as MoS₂²⁵, AsP²⁶, SnSe²⁶ and Janus TMD monolayers²⁷. For example, the d_{22} of SnSe monolayer at -3.5% strain along the armchair direction is up to 628.8 pm/V from unstrained 175.3 pm/V²⁶. Here, the small both biaxial and uniaxial strain (-4% to 4%) effects on piezoelectric properties of monolayer CCC are investigated. The elastic constants C_{66} , piezoelectric coefficients e_{36} and d_{36} as a function of strain are plotted in Figure 2. With both biaxial and uniaxial strains changing from -4% to 4%, both

C_{66} and e_{36} show a non-monotonic behavior. It is found that, according to Equation 5, the compressive strain is in favour of improving piezoelectric response due to reducing C_{66} and improving e_{36} (absolute value). However, the enhancement is very small, and at -2% biaxial (-4% uniaxial) strain, the d_{36} becomes -0.067 (-0.074) pm/V from unstrained -0.065 pm/V, increased only by 3.1% (13.9%).

IV. PIEZOELECTRIC PROPERTIES OF CCB MONOLAYER

A pentagonal CCB monolayer has also been predicted², which can also be viewed as a B-C-B sandwich trilayer. In other words, the C atoms of the first and third layers of penta-graphene are replaced by B atoms. The $P\bar{4}2_1m$ symmetry still holds for CCB monolayer, and our optimized lattice constants $a=b=3.933$ Å, which agrees well with previous ones². The calculated piezoelectric coefficients are $e_{36}=-0.372 \times 10^{-10}$ C/m and $d_{36}=-0.418$ pm/V, which are very larger than ones of CCC monolayer. However, our calculated elastic stiffness coefficients ($C_{11}=86.78$ Nm⁻¹, $C_{12}=87.86$ Nm⁻¹ and $C_{66}=89.20$ Nm⁻¹) violate the Born criteria of mechanical stability^{28,29}:

$$C_{11}C_{22} - C_{12}^2 > 0 \text{ and } C_{66} > 0 \quad (6)$$

Experimentally, Janus TMD monolayer MoSSe with sandwiched S-Mo-Se structure has been synthesized by replacing the top S atomic layer in MoS₂ with Se atoms¹³. Thus, it is possible to build CCB monolayer by replacing the top C (B) atomic layer in monolayer CCC (CBB) with B (C) atoms. The schematic structure of CCB monolayer is shown in Figure 3. The symmetry of CCB monolayer reduces to $Cmm2$ (space group number 35), and the corresponding point group is $mm2$. The Equation 3 changes into:

$$\begin{pmatrix} 0 & 0 & 0 \\ 0 & 0 & 0 \\ e_{31} & e_{32} & 0 \end{pmatrix} = \begin{pmatrix} 0 & 0 & 0 \\ 0 & 0 & 0 \\ d_{31} & d_{32} & 0 \end{pmatrix} \begin{pmatrix} C_{11} & C_{12} & 0 \\ C_{12} & C_{22} & 0 \\ 0 & 0 & C_{66} \end{pmatrix} \quad (7)$$

Here, the d_{31} and d_{32} are derived by Equation 7:

$$d_{31} = \frac{C_{22}e_{31} - C_{12}e_{32}}{C_{11}C_{22} - C_{12}^2} \quad (8)$$

$$d_{32} = \frac{C_{11}e_{32} - C_{12}e_{31}}{C_{11}C_{22} - C_{12}^2} \quad (9)$$

Fortunately, the CCB monolayer also possesses only out-of-plane piezoelectric effect. These also imply that the piezoelectric effects of CCB monolayer can be induced with a uniaxial strain being applied along x or/and y direction, which is different monolayer CCC and CBB with shear strain.

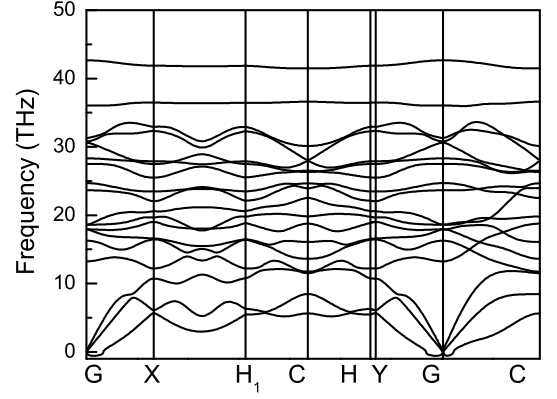


FIG. 4. The phonon band dispersion of CCB monolayer.

Compared with tetragonal structure of CCC and CBB, the crystal structure of CCB changes into orthorhombic, and the optimized lattice constants $a=b=3.771$ Å and $\gamma=92.107^\circ$. To confirm the dynamic stability of CCB monolayer, the phonon spectrum are calculated by VASP+Phonopy code with a supercell of $4 \times 4 \times 1$ using the finite displacement method³⁰. Figure 4 shows the calculated phonon spectrum. Although there are some negligibly small imaginary frequencies near the G point due to calculation error, no imaginary frequencies in the other q points throughout the Brillouin zone are observed, which implies the dynamic stability of CCB monolayer. The mechanical stability of CCB monolayer can be examined by elastic constants C_{ij} . The calculated $C_{11}=142.36$ Nm⁻¹, $C_{22}=193.07$ Nm⁻¹, $C_{12}=34.40$ Nm⁻¹ and $C_{66}=61.71$ Nm⁻¹, which satisfy the Born criteria of mechanical stability^{28,29}. The Young's modulus $C_{2D}(\theta)$ and Poisson's ratio $\nu(\theta)$ as a function of in-plane θ can be attained on the basis of the elastic constants, as follows²⁸:

$$C_{2D}(\theta) = \frac{C_{11}C_{22} - C_{12}^2}{C_{11}\sin^4\theta + A\sin^2\theta\cos^2\theta + C_{22}\cos^4\theta} \quad (10)$$

$$\nu(\theta) = \frac{C_{12}\sin^4\theta - B\sin^2\theta\cos^2\theta + C_{12}\cos^4\theta}{C_{11}\sin^4\theta + A\sin^2\theta\cos^2\theta + C_{22}\cos^4\theta} \quad (11)$$

In which $A = (C_{11}C_{22} - C_{12}^2)/C_{66} - 2C_{12}$ and $B = C_{11} + C_{22} - (C_{11}C_{22} - C_{12}^2)/C_{66}$. We show the calculated $C_{2D}(\theta)$ and $\nu(\theta)$ in Figure 5. Both the Young's modulus $C_{2D}(\theta)$ and Poisson's ratio $\nu(\theta)$ show mechanical anisotropy. According to calculated $C_{2D}(\theta)$, CCB monolayer is softer along the x than y direction, which is due to B-B bond along x direction and C-C bond along y direction. A high Young's modulus implies that the material is rigid, and the calculated results show that strain can easily tune its physical properties along x direction. It is found that the Poisson's ratio ν along x direction (0.179) is smaller than one along y direction (0.242).

A 2D material with piezoelectricity not only should break inversion symmetry, but also has a band gap. The energy band structures of CCB along with CCC and CBB

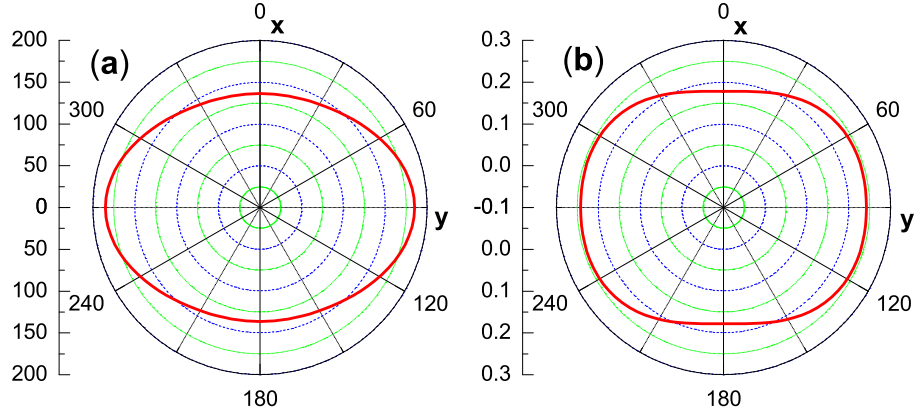


FIG. 5. (Color online) The Young's modulus and Poisson's ratio of CCB monolayer as a function of the angle θ .

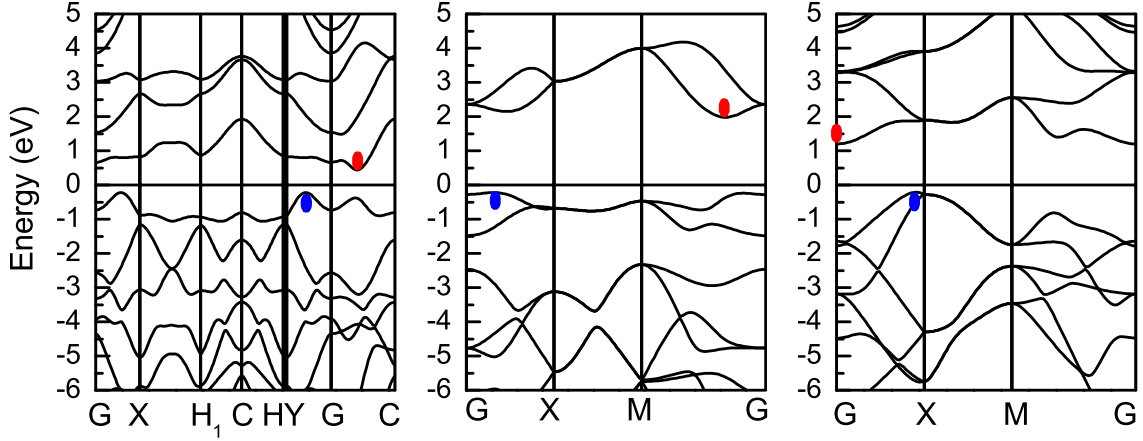


FIG. 6. (Color online) The energy band structures of monolayer CCB (Left), CCC (Middle) and CBB (Right) using GGA, and the VBM and CBM are marked by blue and red ellipses, respectively.

are plotted in Figure 6. It is clearly seen that CCB is an indirect band-gap semiconductor with a band gap of 0.66 eV, which is smaller than indirect gap 2.20 eV of CCC or 1.41 eV of CBB. The valence band maximum (VBM) lies on the G-Y path, while the conduction band minimum (CBM) is located on the G-C path. In fact, the valence band extrema (VBE) along G-X path is very close to VBM due to γ being very close to 90, and the difference is less than 1 meV. The carrier mobility of a semiconductor is an important factor for the application of electron device. The carrier mobility of a 2D material (μ_{2D}) by the deformation potential (DP) theory proposed by Bardeen and Shockley³¹ is defined as:

$$\mu_{2D} = \frac{e\hbar^3 C_{2D}}{K_B T m^* m_d E_l^2} \quad (12)$$

where T , m^* and m_d ($\sqrt{m_x m_y}$) are the temperature, the effective mass in the transport direction and the average effective mass. The C_{2D} is the Young's modulus derived from elastic constants C_{ij} . In addition, E_l is the DP constant defined by $E_l = \Delta E / \delta$ ($\delta = \Delta l / l_0$), where ΔE is the energy shift of the band edge of CBM or VBM

with respect to the vacuum level after applying uniaxial strain. After attaining μ_{2D} , the relaxation time τ can be attained by:

$$\tau = \mu_{2D} m^* / e \quad (13)$$

According to DP theory, the rectangular supercell is used to calculate carrier mobilities of monolayer CCB along the x and y directions in Figure 3. The calculated effective masses for electrons (CBM) and holes (VBM) with GGA are shown in Table III. The band energies of the VBM and CBM with respect to the vacuum energy as a function of $\Delta x/x$ and $\Delta y/y$ are plotted in Figure 7, and the DP constant E_l is calculated by linearly fitting these data. The carrier mobility and relaxation time for the electrons and holes of monolayer CCB on the basis of the calculated effective mass, elastic constant, and deformation potential constant are calculated along x and y directions at 300 K, which are summarized in Table III. It is found that the electron mobility along y direction ($8865.23 \text{ cm}^2 \text{V}^{-1} \text{s}^{-1}$) is almost 97 times larger than that along x direction ($91.92 \text{ cm}^2 \text{V}^{-1} \text{s}^{-1}$). However, the hole mobilities along both

TABLE III. For CCB monolayer, elastic modulus (C_{2D}), effective mass (m^*), deformation potential (E_l), carrier mobility (μ_{2D}) and relaxation time (τ) at 300 K.

| Carrier type | | C_{2D} (Nm $^{-1}$) | m^* | E_l (eV) | μ_{2D} (cm 2 V $^{-1}$ s $^{-1}$) | τ (s) |
|--------------|---|------------------------|-------|------------|---|------------------------|
| Electrons | x | 136.23 | 1.57 | 5.00 | 91.92 | 8.18×10^{-14} |
| | y | 184.76 | 0.42 | -1.15 | 8865.23 | 2.10×10^{-12} |
| Holes | x | 136.23 | -0.45 | -9.20 | 114.63 | 2.90×10^{-14} |
| | y | 184.76 | -1.02 | 6.97 | 118.75 | 7.46×10^{-14} |

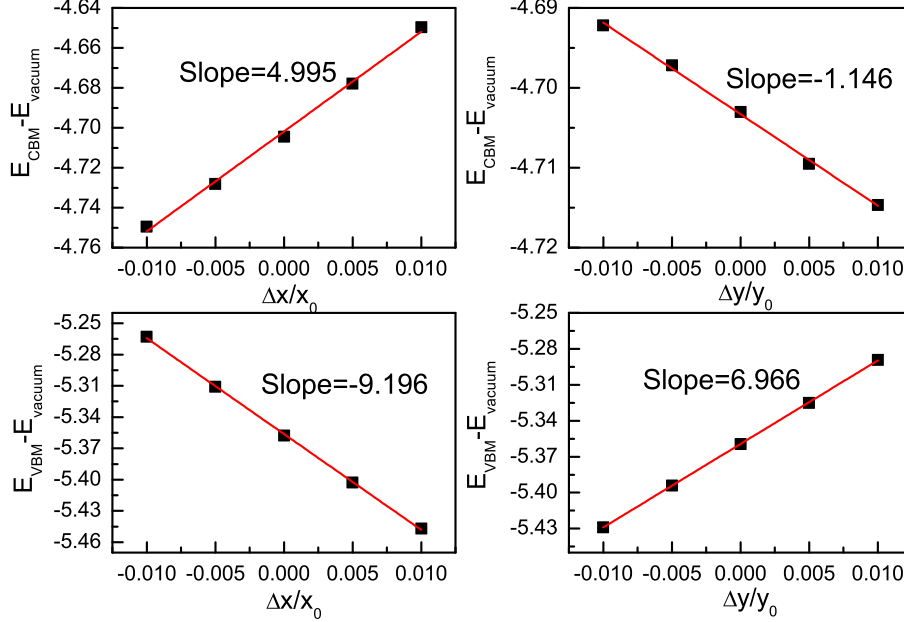


FIG. 7. (Color online) With respect to the vacuum energy, the band energies of the VBM and CBM of CCB monolayer as a function of lattice dilation along both x and y directions. The red solid lines are linear fitting curves, and the fitted slopes are given, corresponding to the DP.

x (114.63 cm 2 V $^{-1}$ s $^{-1}$) and y (118.75 cm 2 V $^{-1}$ s $^{-1}$) directions are very low, which is close to electron mobility along x direction.

In fact, the CCB is a representative Janus monolayer. The asymmetric along the z direction with respect to central C atomic layer results in an out-of-plane piezoelectricity. However, mirror symmetry along x and y directions gives rise to disappeared in-plane piezoelectricity. This means that an in-plane stress or strain can only induce a polarization change vertical to the plane. Based on calculated C_{ij} and e_{ij} , the out-of-plane piezoelectric strain coefficient d_{31} and d_{32} can be attained, and the corresponding values are -0.505 pm/V and 0.273 pm/V, respectively. The out-of-plane d_{31} is obviously higher than out-of-plane ones of many other 2D materials, such as functionalized h-BN (0.13 pm/V)³², MoSSe (0.29 pm/V)³³, SbTeI (-0.37 pm/V)³⁴, MoSTe (0.4 pm/V)³⁵, Janus group-III materials (0.46 pm/V)³⁶ and α -In $_2$ Se $_3$ (0.415 pm/V)³⁷. It is lower than one of BiTeI (-0.66 pm/V)³⁴, Sc $_2$ CO $_2$ (0.78 pm/V)³⁸ or La $_2$ CO $_2$ (0.65 pm/V)³⁸. However, the monolayer BiTeI, Sc $_2$ CO $_2$ or La $_2$ CO $_2$ not only has out-of-plane piezoelectricity, but

also has in-plane piezoelectricity. Some related data are summarized in Table II. Although the d_{36} (CCC monolayer) and d_{31} or d_{32} (CCB monolayer) are all related to the out-of-plane piezoelectric effects, they are obviously different. The d_{36} represents the piezoelectric response between the out-of-plane polarization and the in-plane shearing deformation, while d_{31} or d_{32} is referred to as the coupling between the out-of-plane polarization and the in-plane normal strain.

V. CONCLUSION

In summary, the related piezoelectric effects of CCC monolayer are studied by using reliable first-principles calculations. Due to special symmetry for CCC monolayer, only out-of-plane d_{36} exists, but it is very small. Firstly, we use both biaxial and uniaxial strains to tune piezoelectric properties of CCC monolayer. At -2% biaxial (-4% uniaxial) strain, the d_{36} is increased only by 3.1% (13.9%), and the enhancement is very small. Inspiring from the already synthesized MoSSe monolayer,

a Janus CCB monolayer with dynamic and mechanical stability is constructed, and the asymmetric along the z direction and mirror symmetry along x and y directions induce pure out-of-plane piezoelectricity. It is also found that CCB monolayer is a semiconductor, which is necessary for piezoelectric application. The calculated d_{31} and d_{32} are -0.505 pm/V and 0.273 pm/V, respectively, and the out-of-plane piezoelectric effect are obviously improved, compared with d_{36} of CCC monolayer. The out-of-plane piezoelectricity d_{31} of CCB monolayer is higher compared with other many 2D known materials. The very high room-temperature electronic mobility (8865.23 cm²V⁻¹s⁻¹) along y direction is predicted, which is very higher than that of Si (about 1400

cm²V⁻¹s⁻¹). Our works not only supply an experimental proposal for achieving large pure out-of-plane piezoelectric effect, but also offer an insight into piezoelectric effect of penta-graphene.

ACKNOWLEDGMENTS

This work is supported by the Natural Science Foundation of Shaanxi Provincial Department of Education (19JK0809). We are grateful to the Advanced Analysis and Computation Center of China University of Mining and Technology (CUMT) for the award of CPU hours and WIEN2k/VASP software to accomplish this work.

- ¹ S. Zhang, J. Zhou, Q. Wang, X. Chen, Y. Kawazoe and P. Jena, Proc. Natl. Acad. Sci. Unit. States Am. **112**, 2372 (2015).
- ² F. Li, K. Tu, H. Zhang and Z. Chen, Phys. Chem. Chem. Phys. **17**, 24151 (2015).
- ³ Y. Ma, L. Kou, X. Li, Y. Dai and T. Heine, NPG Asia Mater. **8**, e264 (2016).
- ⁴ J. Li, X. Fan, Y. Wei, H. Liu, S. Li, P. Zhao and G. Chen, Sci. Rep. **6**, 33060 (2016).
- ⁵ H. Sun, S. Mukherjee and C. V. Singh, Phys. Chem. Chem. Phys. **18**, 26736 (2016).
- ⁶ F. Q. Wang, J. Yu, Q. Wang, Y. Kawazoe and P. Jena, Carbon **105**, 424 (2016).
- ⁷ W. Xu, G. Zhang and B. Li, J. Chem. Phys. **143**, 154703 (2015).
- ⁸ J. Sun, Y. G. Guo, Q. Wang and Y. Kawazoe, Carbon **145**, 445 (2019).
- ⁹ L. L. Liu, Y. Wang, C. P. Chen, H. X. Yu, L. S. Zhao and X. C. Wang, RSC Adv. **7**, 40200 (2017).
- ¹⁰ W. Wu and Z. L. Wang, Nat. Rev. Mater. **1**, 16031 (2016).
- ¹¹ W. Wu, L. Wang, Y. Li, F. Zhang, L. Lin, S. Niu, D. Chenet, X. Zhang, Y. Hao, T. F. Heinz, J. Hone and Z. L. Wang, Nature **514**, 470 (2014).
- ¹² H. Zhu, Y. Wang, J. Xiao, M. Liu, S. Xiong, Z. J. Wong, Z. Ye, Y. Ye, X. Yin and X. Zhang, Nat. Nanotechnol. **10**, 151 (2015).
- ¹³ A. Y. Lu, H. Zhu, J. Xiao, C. P. Chuu, Y. Han, M. H. Chiu, C. C. Cheng, C. W. Yang, K. H. Wei, Y. Yang, Y. Wang, D. Sokaras, D. Nordlund, P. Yang, D. A. Muller, M. Y. Chou, X. Zhang and L. J. Li, Nat. Nanotechnol. **12**, 744 (2017).
- ¹⁴ L. Dong, J. Lou and V. B. Shenoy, ACS Nano, **11**, 8242 (2017).
- ¹⁵ M. N. Blonsky, H. L. Zhuang, A. K. Singh and R. G. Hennig, ACS Nano, **9**, 9885 (2015).
- ¹⁶ R. X. Fei, W. B. Li, J. Li and L. Yang, Appl. Phys. Lett. **107**, 173104 (2015).
- ¹⁷ K. N. Duerloo, M. T. Ong and E. J. Reed, J. Phys. Chem. Lett. **3**, 2871 (2012).
- ¹⁸ Y. Chen, J. Y. Liu, J. B. Yu, Y. G. Guo and Q. Sun, Phys. Chem. Chem. Phys. **21**, 1207 (2019).
- ¹⁹ X. Wu, D. Vanderbilt and D. R. Hamann, Phys. Rev. B **72**, 035105 (2005).
- ²⁰ P. Hohenberg and W. Kohn, Phys. Rev. **136**, B864 (1964); W. Kohn and L. J. Sham, Phys. Rev. **140**, A1133 (1965).
- ²¹ G. Kresse, J. Non-Cryst. Solids **193**, 222 (1995).
- ²² G. Kresse and J. Furthmüller, Comput. Mater. Sci. **6**, **15** (1996).
- ²³ G. Kresse and D. Joubert, Phys. Rev. B **59**, 1758 (1999).
- ²⁴ J. P. Perdew, K. Burke and M. Ernzerhof, Phys. Rev. Lett. **77**, 3865 (1996).
- ²⁵ N. Jena, Dimple, S. D. Behere and A. D. Sarkar, J. Phys. Chem. C **121**, 9181 (2017).
- ²⁶ S. D. Guo, X. S. Guo, Y. Y. Zhang and K. Luo, arXiv:1910.08700 (2019).
- ²⁷ Dimple, N. Jena, A. Rawat, R. Ahammed, M. K. Mohanta and A. D. Sarkar, J. Mater. Chem. A **6**, 24885 (2018).
- ²⁸ E. Cadelano, P. L. Palla, S. Giordano and L. Colombo, Phys. Rev. B **82**, 235414 (2010).
- ²⁹ R. C. Andrew, R. E. Mapasha, A. M. Ukpong and N. Chetty, Phys. Rev. B **85**, 125428 (2012).
- ³⁰ A. Togo, F. Oba, and I. Tanaka, Phys. Rev. B **78**, 134106 (2008).
- ³¹ S. Bruzzone and G. Fiori, Appl. Phys. Lett. **99**, 222108 (2011).
- ³² A. A. M. Noor, H. J. Kim and Y. H. Shin, Phys. Chem. Chem. Phys. **16**, 6575 (2014).
- ³³ S. D. Guo, X. S. Guo, R. Y. Han and Y. Deng, Phys. Chem. Chem. Phys. (2019). DOI: 10.1039/C9CP04590B.
- ³⁴ S. D. Guo, X. S. Guo, Z. Y. Liu, Y. N. Quan, arXiv:1909.13227 (2019).
- ³⁵ M. Yagmurcukardes, C. Sevik and F. M. Peeters, Phys. Rev. B **100**, 045415 (2019).
- ³⁶ Y. Guo, S. Zhou, Y. Z. Bai, J. J. Zhao, Appl. Phys. Lett. **110**, 163102 (2017).
- ³⁷ L. Hu and X. R. Huang, RSC Adv. **7**, 55034 (2017).
- ³⁸ J. Tan, Y. H. Wang, Z. T. Wang et al., Nano Energy **65**, 104058 (2019).